Sensors and Materials, Vol. 37, No. 1 (2025) 93–104
MYU Tokyo

S & M 3893

Laser-induced Plasma Detection for Laser Percussion Drilling of Stainless Steel and CoCrMo Alloy

Yuan-Jen Chang,[1] Chau-Shing Wang,[2*]
G. Siva Durga Manikanta,[3] and Yang-Hung Hsiao[3]

[1]Graduate Institute of Manufacturing Technology, National Taipei University of Technology, No. 1, Sec. 3, Zhongxiao E. Rd., Taipei 10608, Taiwan
[2]Department of Electrical Engineering, National Changhua University of Education, No. 2, Shi-Da Road, Changhua City 500, Taiwan
[3]Department of Mechanical Engineering, National Yunlin University of Science and Technology, No. 123, University Road Section 3, Douliou, Yunlin 640, Taiwan

(Received August 22, 2024; accepted December 4, 2024)

Keywords: laser percussion drilling, laser-induced plasma, micromachining

Laser percussion drilling is a micromachining process for generating a microhole with a diameter of less than 500 μm. The laser beam heated the material to the vaporization temperature, after which a hole was formed. Laser percussion drilling is increasingly used in micromachining. Monitoring the laser drilling process is crucial for improving the quality of drilling. Among the many methods for monitoring laser drilling, such as optics, sound, and vibration, the method of detecting laser-induced plasma with an external electric field has the advantages of being real time, inexpensive, and free from environmental interference. Therefore, in this study, we used a pair of copper electrode plates to generate a strong electric field around the drilling site to apply a voltage of hundreds of volts. The laser-induced plasma interferes with the electric field and generates electrical signals, which are then measured using an RC circuit. From this measured electrical signal, a waveform was observed for each laser shot. In this study, seven different laser energies were used to test the detected plasma signals and to measure the depth and diameter of each drill hole. We also compared the differences in the detected plasma signals when drilling two different materials (stainless steel SUS 304 and a CoCrMo alloy). The curve fitting method was used to derive a mathematical model of the plasma signal vs the number of laser shots of two different materials. Because the thermal conductivity and ablation rate of different materials are different, the coefficients of the curve-fitting results are also different. The experiments and mathematical models in this study are helpful for understanding the responses of different materials to laser drilling.

1. Introduction

Microscale laser processing technology is widely employed and is suitable for a variety of materials, including super hard materials and medical device microstructures.[1–4] It is also

*Corresponding author: e-mail: cswang@cc.ncue.edu.tw
https://doi.org/10.18494/SAM5323

ISSN 0914-4935
https://myukk.org/

utilized for laser cleaning and piercing,[5,6] with micro-drilling being the predominant application (with diameters less than 0.1 mm). If a mechanical drill is employed, significant tool wear and drilling-chip removal are inevitable. Therefore, noncontact laser percussion drilling can overcome these challenges. However, there are numerous laser control parameters (such as current, frequency, pulse width, power, focal length, and auxiliary gas), and the interaction relationship with the material to be treated is complex. As a result, several monitoring methods have been employed to monitor laser processing to determine suitable processing parameters. At present, in industrial applications, monitoring can be carried out in several ways, such as by exploring the state of laser drilling through sound signals and using the collection of photoacoustic signals of the circuit board when the laser stably removes materials.[7] The sound signal also varied when the laser processing energy was altered. These phenomena were compared with the volume of material removed following laser ablation.[8] The sound signal monitoring method can quickly determine the processing state of hard materials, but it can easily fail to receive signals for soft or sound-absorbing materials. Light can also be used as a signal collection item.[9] In early circuit board drilling, materials with different characteristics were used to generate high-intensity reflected light when the laser hit a copper foil. This reflected light is fed back to the light sensor to measure the light intensity and determine where the laser drilling focus position is. In addition, by analyzing the strong light generated during laser processing, the entrance or bottom size of the lower hole can be determined, which can be used for continuous laser drilling to record the geometry of the hole after each laser shot.[10] High-speed charge-coupled device (CCD) cameras are used to monitor module laser processing and to determine the depth of the hole by calculating the pixels of the image captured by cameras.[11] In another paper, a new sensing technique is described in which during laser keyhole welding, an electrically separated welding nozzle acts as a passive electric probe to measure the charge potential in the area between the nozzle and the workpiece.[12] However, this type of technique has a lower efficiency than that with an applied electric field. The study of electric fields for monitoring laser-induced plasmas has also been reported.[13] It has been determined that the recitation of laser-induced plasma with a high-voltage discharge can increase the signal intensity, thereby increasing the signal-to-noise ratio and reducing the detection limit of laser-induced plasma.[14] Nassef and Ali[15] discovered that the signal intensity enhancement factor increased as the spark discharge voltage increased in spark-discharge-assisted laser-induced breakdown spectroscopy (LIBS) and conventional LIBS. Furthermore, in both spark-discharge-assisted LIBS and conventional LIBS, the plasma temperature remained constant. The effect of a static electric field on laser-induced plasma revealed an increase in signal intensity and a small decrease in electron number density while the plasma temperature remained constant.[16] As shown in Ref. 17, a low-voltage and high-current arc discharge technique combined with LIBS resulted in increased plasma plume persistence as well as signal intensity enhancement. As described in Ref. 18, in the presence of an external electric field, the plasma parameters remained constant for a few microseconds after plasma generation, which can be used by LIBS for a more accurate quantitative analysis of any material. In the presence of an external electric field, fluctuations in the laser-induced plasma were observed, which increased the plasma decay time and, as a result, the signal intensity. By increasing the average grain size number, a

transverse E-field with and without side airflow effectively refined the grains of the heat-affected zone (HAZ) near the fusion zone of a through hole.[19] Ren *et al.*[20] reported that according to the theoretical and experimental results of drilling titanium sheets with ANSYS parametric design language (APDL) and ANSYS software's life and death technology, depth and diameter could be increased by increasing the number of laser pulses and laser energy with some defects. In our previous work,[21,22] the laser drilling of stainless steel was monitored using a pair of flat or interdigitated electrodes supplied at hundreds of volts. The laser-induced plasma intensity was measured using the electrodes.

Hard stainless steel (SUS 304) is not suitable for mechanical microdrilling; therefore, laser percussion drilling is mostly used. In addition to SUS 304, cobalt-chromium-molybdenum alloys (CoCrMo alloys) were tested in the experiment. CoCrMo alloys are widely used in medical implant devices, such as knee implant materials. CoCrMo alloys are particularly suitable for alloys with high hardness, high polish, and extremely wear-resistant materials. In this study, laser percussion drilling and monitoring were conducted for these two materials.

2. Experimental Setup

In this study, a pulsed fiber laser (YLPN-2-20×500-200) with a pulse energy range of 0.5–2 mJ, a wavelength of 1064 nm, a repetition frequency of 40 kHz, and a pulse width of 250 ns was used to generate laser pulses. The method for detecting laser-induced plasma generated during laser microdrilling used a pair of copper electrode plates to monitor the plasma. A voltage of hundreds of volts was applied to the electrode plates to establish a stable high-voltage electric field between them. The charged ions in the laser-induced plasma passed through the electric field between the electrode plates to generate an electric current. Finally, a detection circuit was used to capture and convert the current signal into a voltage signal. The strength of the plasma could be observed using this voltage signal. Figure 1 shows the schematic of the experimental setup. When the laser beam hits the stainless steel material, the material instantly ionizes owing to high-energy density ablation, causing plasma ions to splash upward. When these plasma ions fly past the electrode plates with an electric field, the positive ions will be attracted to the negative electrode plate, and the negatively charged ions will fly towards the positive electrode plate. Therefore, a current is generated in the detection circuit, and this current passes through a resistor to generate a voltage, which is the detected plasma signal.

SUS 304 stainless steel workpieces with dimensions of 30 × 30 × 2 mm^3 and or CoCrMo alloy workpieces with a diameter of 30 mm and a thickness of 2 mm were processed. The material properties are listed in Table 1. The surface roughness of the materials was measured to be *R*a 0.07 nm. Before laser processing, the workpieces were cleaned using an ultrasonic cleaning machine with acetone, ethanol, and distilled water for 20 min each.

Seven different laser pulse energies (0.5, 0.75, 1, 1.25, 1.5, 1.75, and 2 mJ) and three different external voltages (350, 400, and 450 V) for electrode plates were employed as experimental parameters. A laser power meter was used to measure the output energy of the laser machine to ensure the accuracy of the laser energy. Electrode plates with dimensions of 35 × 5 × 1 mm^3 were positioned on both sides of the laser-drilling hole separated by a distance of 2 mm, as

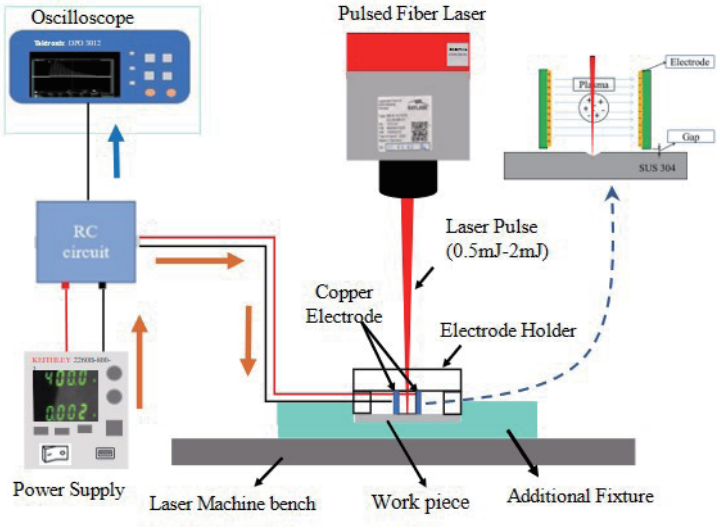

Fig. 1. (Color online) Schematic of experimental setup of real-time plasma detection for laser micro-drilling.

Table 1
Material properties of SS304 and CoCrMo.

Properties	SUS 304	CoCrMo alloy
Density (g/cm^3)	8	8.55
Thermal expansion (μm/m-K)	17.3	11.2
Thermal conductivity (W/m-K)	16.2	6.5
Electrical resistivity (Ohm-cm)	7.20×10^{-5}	9.86×10^{-5}
Melting point (°C)	1455	1440

shown in the upper right of Fig. 1. The two electrodes were utilized to detect laser-induced plasma during the laser microdrilling of the materials.

The experiments for each set of processing parameters were repeated thrice to ensure data stability. Each set of parameters was processed using 40 laser shots. To ensure consistent positioning between the electrodes, an additional workpiece support device was fixed to the laser machine table. This setting fixed the position of the workpiece on the laser machine table, ensuring that each laser shot occurred at the same location. During the laser experiment, the height of the laser z-axis remained unchanged. For the consistency of the experiment, it must be checked before each experiment whether the laser beam hits the middle of the two electrode plates.

3. Experimental Results and Discussion

3.1 Detected laser-induced plasma

Figure 2 shows the laser-induced plasma detected on an oscilloscope when SUS 304 and CoCrMo alloy materials were drilled by 40 laser shots using 2 mJ energy and 450 V electrode plates. The recorded signal showed 40 peaks, representing 40 laser pulses. The first few shots of

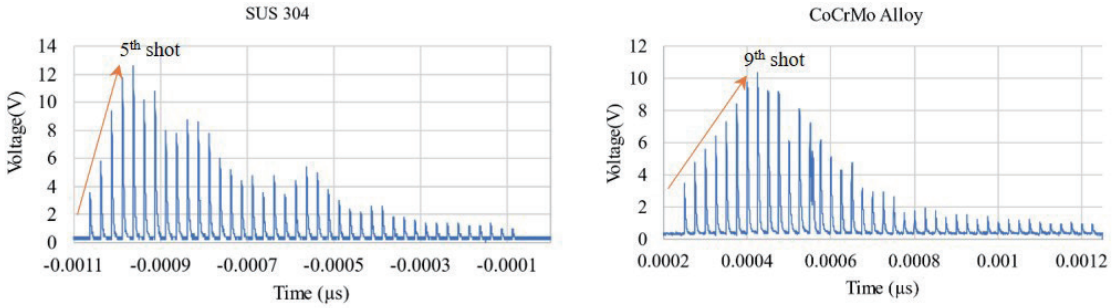

(a) (b)

Fig. 2. (Color online) Captured plasma signals: (a) SUS 304 and (b) CoCrMo.

the laser cause the material to rapidly heat up, resulting in more ablation and more plasma being generated; thus, the detected pulse increases rapidly. However, as the depth of the hole increased, the plasma ions fly farther to the electrode plates. The longer flight distance means that more positive and negative ions neutralize each other, resulting in less plasma signal detection. In addition, the plasma of a deeper hole flies at a straighter angle when ejected from the hole bottom, so the plasma signal that can be detected is weaker. Compared with shallower holes in the early stages of drilling, the plasma generated can splash laterally, so stronger signals can be detected. Notably, it can be observed that SS304 has a maximum peak at the 5th shot of the laser with a steeper rising slope compared with the CoCrMo alloy at the 9th shot, owing to the higher thermal conductivity of SUS 304.

3.2 Measurement of hole diameter and depth

The diameter and depth measurements were conducted separately. The depth was measured using a white-light interferometer (WIM-1510MS) for shallow holes with depths of less than 25 μm, as depicted in Fig. 3. However, owing to the scanning range limitations of the white-light interferometer, a tool microscope (OLYMPUS U-PMTVC) was utilized to measure depths greater than 25 μm. This depth measurement was achieved by enlarging the holes using a microscope and focusing on the bottom of the hole from the surface of the workpiece. The current depth of the hole was then measured using a numerical reading meter. To confirm the efficiency of the depth measured using a numerical reading meter in an optical microscope, we cut the hole into half, as shown in Fig. 4. It was found that the error percentage of the depth measured from the profile and depth measurements with the optical microscope was small.

On the other hand, the diameter measurements used Mosaic V 2.1 software to draw a three-point circle to estimate the hole diameter. The locations of these three points must be selected at the junction of the circumference of the crater and the slag in the holes.

3.3 Comparisons of hole diameters and depths of different laser energies

Figures 5 and 6 show the drilling depth and diameter, respectively, for both materials. The hole depth increases almost linearly with the number of laser shots. The higher the laser energy,

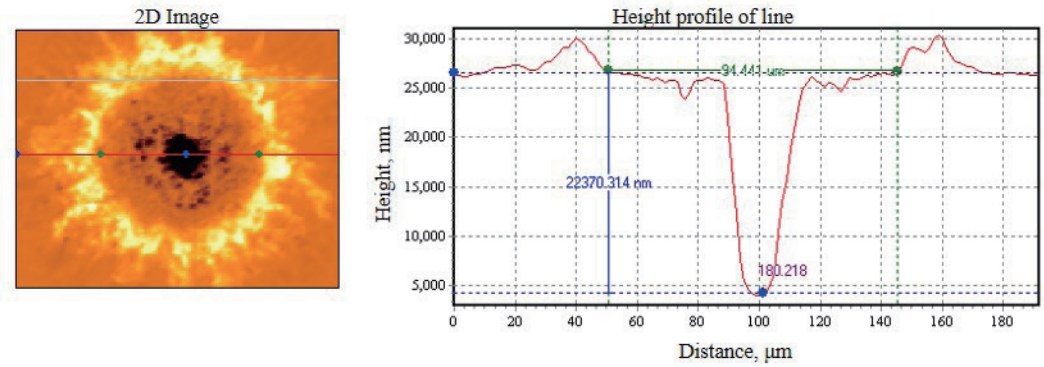

Fig. 3. (Color online) Depth and diameter measurement in white-light interferometer (5 shots).

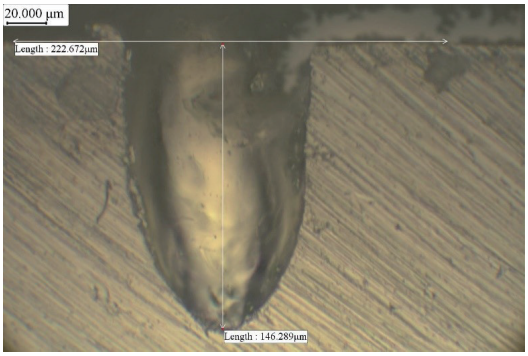

Fig. 4. (Color online) Cross section of a drilling hole.

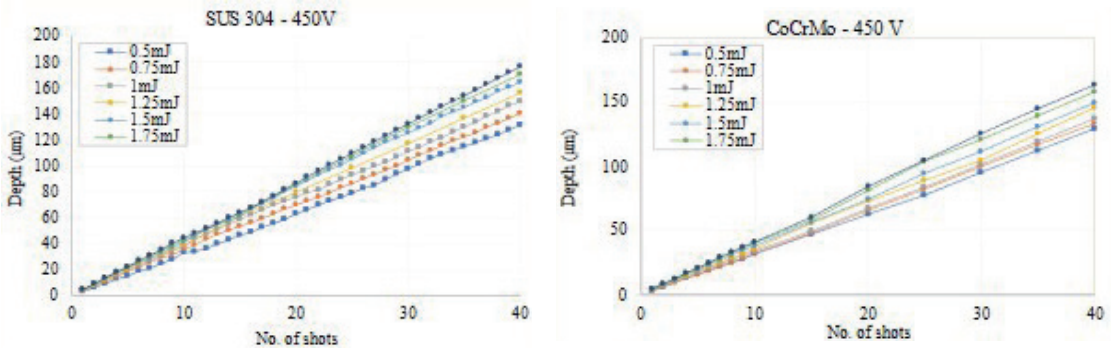

Fig. 5. (Color online) Comparison of depths of two materials.

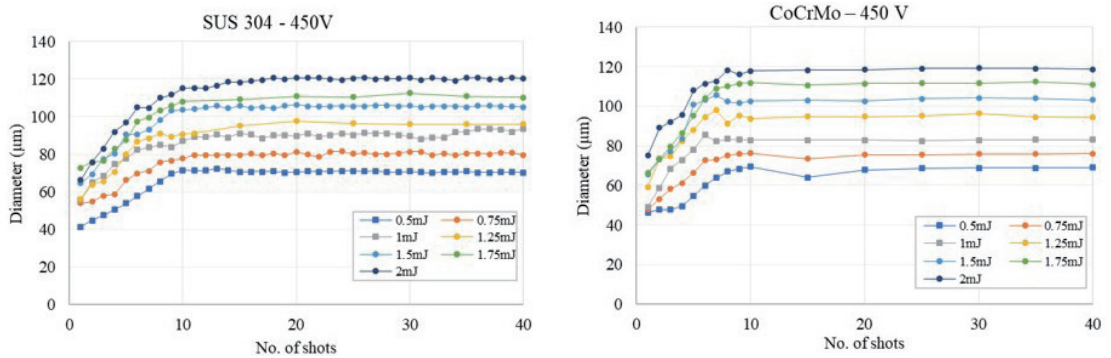

Fig. 6. (Color online) Comparison of diameters of two materials.

the higher the slope of the hole depth. On the other hand, the diameter stops increasing once it reaches a certain width. Additionally, SUS 304 has greater depth and diameter than the CoCrMo alloy.

3.4 Comparison of detected plasma signals of different electrode voltages and laser energies

The plasma signals captured by the oscilloscope are stored as CSV data files, and then the peak value of each pulse is found using the MATLAB program. Therefore, the peak value of each pulse in Fig. 2 is expected to appear at each point in Fig. 7. In the figure, the detected plasma signals of seven different laser energies (0.5, 0.75, 1, 1.25, 1.5, 1.75, and 2 mJ) of the electrode at 450 V are compared. It can be observed that the stronger the laser energy, the more material is ablated, thus creating more plasma.

Figure 8 shows a comparison between three different electrode voltages (350, 400, and 450 V) for a laser pulse energy of 2 mJ. It can be observed that higher electrode voltages result in higher detection peaks owing to the presence of a strong electric field between the electrodes.

During laser drilling, SUS 304 stainless steel melts more easily than the CoCrMo alloy because of its higher electrical and thermal conductivities. Therefore, laser processing produces a larger plasma plume for SUS 304 than for the CoCrMo alloy, making laser ablation easier and signal peak appearance earlier, as shown in Fig. 9. The lower electrical and thermal conductivities of the CoCrMo alloy resulted in lower signal detection and lower depth and diameter measurements.

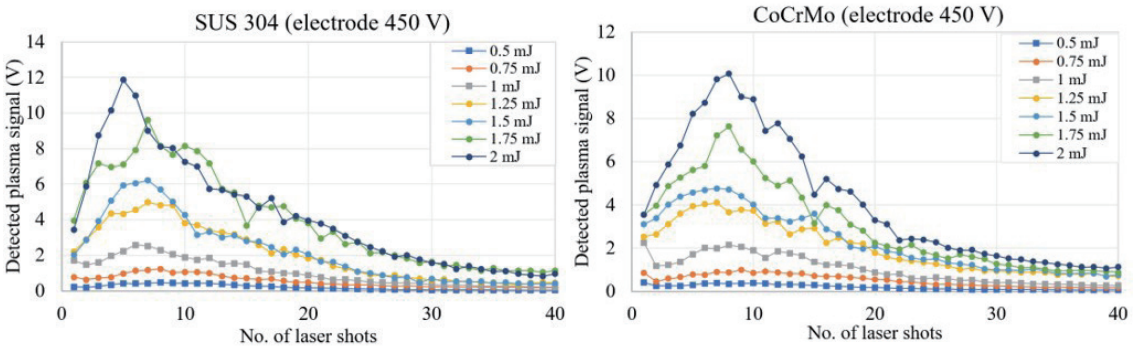

Fig. 7. (Color online) Comparison of detected plasma signals of different laser energies for both materials.

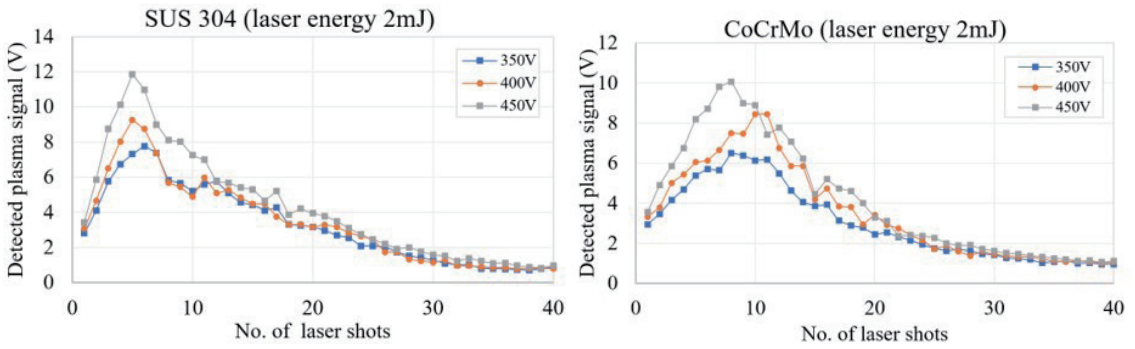

Fig. 8. (Color online) Comparison of detected plasma signals of different electrode voltages for both materials.

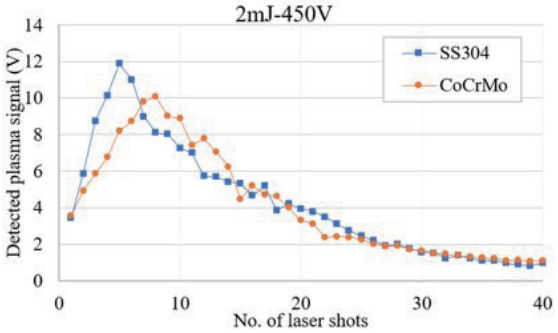

Fig. 9. (Color online) Comparison of detected plasma signals of both materials.

3.5 Curve fitting

The relationship between the detected plasma signal and the number of laser shots was evaluated through curve fitting using the MATLAB numerical analysis software. The formula used for this analysis is[23]

$$f(x) = axe^{-bx} + c. \tag{1}$$

The *a*, *b*, and *c* values are correlated to the detected peaks of the plasma signal, where "*a*" relates to the rising speed of the curve, "*b*" is the decaying speed of the curve, "*c*" determines the last peak value, "*x*" is the number of laser shots, and *f*(*x*) is the detected plasma signal of the xth laser shot. The curve fitting of the 450 V electrode voltage and 2 mJ of laser energy for both materials is shown in Fig. 10.

Curve fitting was conducted for all combinations of the three electrode voltages (350, 400, 450 V) and seven laser energies, as shown in Table 2. The R^2 values in all fitting results were above 0.95, which shows that the degree of fitting was high.

From the data in Fig. 11, it is evident that SUS 304 consistently exhibits a larger "*a*" value than the CoCrMo alloy in all experiments. This difference can be attributed to the higher maximum detection peak observed for SUS 304. Therefore, we believe that a larger "*a*" value indicates a higher material removal rate for SUS 304. Notably, SUS 304 has a higher thermal conductivity than the CoCrMo alloy.

Figure 12 shows that the CoCrMo alloy exhibits larger "*b*" values for the 0.5 mJ laser pulse energy. However, at higher pulse energies, the "*b*" value of SUS 304 was higher. Furthermore, SUS 304 consistently achieved deeper holes than the CoCrMo alloy under the same parameters. This can be attributed to the longer plasma-to-electrode distance of SUS 304. Therefore, recombinations and reactions are more likely to occur during plasma-ion flight, causing the signal to decay faster.

As shown in Fig. 13, the coefficient "*c*" is related to the detection signal limit. The higher the "*c*" value, the stronger the ability to detect more laser shots of plasma. This coefficient was not affected by the material properties, as evidenced by the absence of any clear trend in the figure. However, after examining the error bars, it is clear that "c" increases with the laser pulse energy.

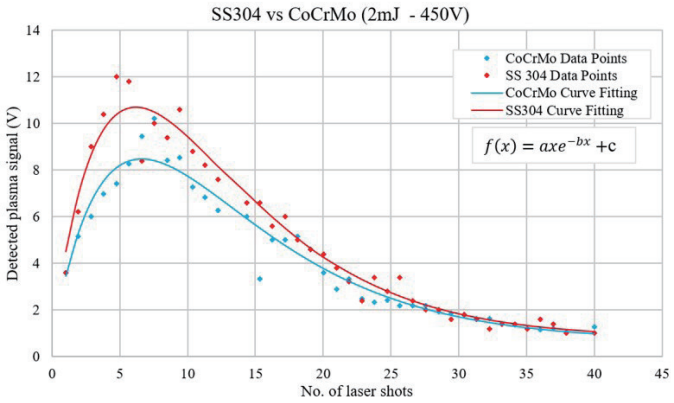

Fig. 10. (Color online) Curve fitting of both materials.

Table 2
Comparison of curve fitting coefficients of SUS 304 and CoCrMo alloy.

Voltage (V)	Laser energy (mJ)	*a* SUS	*a* CoCrMo	*b* SUS	*b* CoCrMo	*c* SUS	*c* CoCrMo	R^2 SUS	R^2 CoCrMo
	0.5	0.1207	0.1188	0.1328	0.1611	−0.01638	0.05038	0.9634	0.9574
	0.75	0.3712	0.2766	0.1502	0.1456	0.01362	0.1061	0.9534	0.9668
	1	0.7256	0.5885	0.1733	0.1632	0.196	0.2113	0.9361	0.9752
350	1.25	1.135	0.9353	0.1691	0.1516	0.4614	0.492	0.9449	0.9672
	1.5	1.774	1.243	0.1584	0.1544	0.1303	0.5422	0.9717	0.9704
	1.75	2.697	1.569	0.1701	0.1412	0.9993	0.4325	0.9902	0.9638
	2	2.708	2.145	0.1578	0.1416	0.5974	0.5347	0.9713	0.9643
	0.5	0.1301	0.1198	0.1218	0.1606	−0.04203	0.05495	0.9537	0.956
	0.75	0.3891	0.298	0.1536	0.1436	0.02009	0.1058	0.9544	0.9794
	1	0.7618	0.6353	0.164	0.1553	0.1621	0.1915	0.9115	0.9798
400	1.25	1.906	1.186	0.1922	0.1616	0.17236	0.5383	0.9674	0.9685
	1.5	2.017	1.554	0.1603	0.1551	0.1865	0.5148	0.9789	0.9715
	1.75	3.062	2.302	0.1773	0.1472	1.153	0.1896	0.9852	0.9567
	2	3.169	2.606	0.1734	0.1388	0.835	0.2377	0.9291	0.9531
	0.5	0.1735	0.1349	0.1425	0.155	−0.01276	0.04818	0.9621	0.9649
	0.75	0.3995	0.3041	0.1521	0.1348	0.115	0.08815	0.9409	0.98
	1	0.9888	0.7694	0.1708	0.1556	0.1923	0.1817	0.959	0.9718
450	1.25	1.963	1.46	0.1616	0.1614	0.2073	0.6474	0.9876	0.9783
	1.5	2.449	1.854	0.1734	0.1712	0.2016	0.7659	0.9585	0.976
	1.75	3.274	2.514	0.1588	0.1592	0.7933	0.6141	0.9651	0.9557
	2	4.306	3.445	0.1817	0.1502	1.032	0.3715	0.9531	0.9644

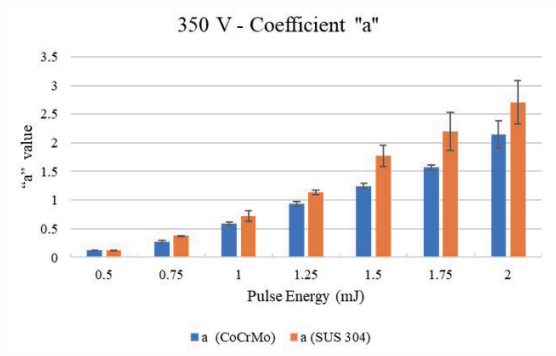

Fig. 11. (Color online) Comparison of coefficient "*a*" values.

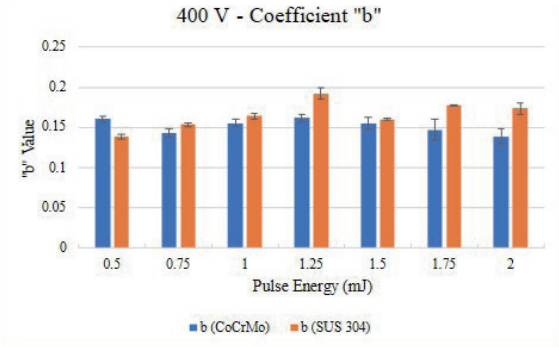

Fig. 12. (Color online) Comparison of coefficient "*b*" value.

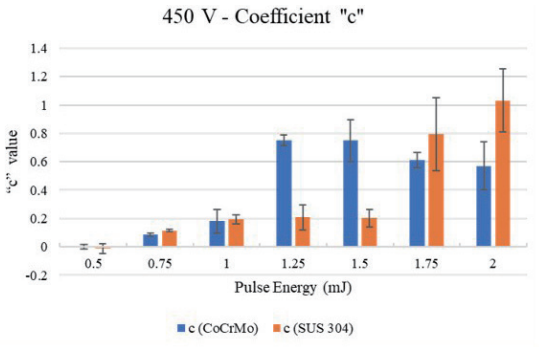

Fig. 13. (Color online) Comparison of coefficient "*c*" value.

4. Conclusion

Compared with SUS 304, the CoCrMo alloy has a higher melting point and is more resistant to ablation. In the experiment with the CoCrMo alloy, the detected plasma signal induced by each laser shot increased more slowly, and more laser shots were required to rise to the highest value. Because of its lower thermal conductivity, laser processing produces smaller plasma plumes. The characteristic differences in the laser ablation process of these two materials can be observed in Figs. 2 and 9. From the curve fitting, the coefficient "*c*" has no significant relationship with the two materials. The coefficients "*a*" and "*b*" are related to material properties and can be used to distinguish different materials with different properties. Furthermore, they can be used to determine the relationship between the hole depth, diameter, and detected plasma signal. The laser microdrilling monitoring technique for different materials can be developed.

Acknowledgments

This work was supported by the National Science and Technology Council of Taiwan, NSTC 111-2221-E-018-015.

References

1 B. Mills, D. J. Heath, M. Feinaeugle, J. A. Grant-Jacob, and R. W. Eason: J. Laser Appl. **26** (2014) 041501. https://doi.org/10.2351/1.4893749
2 J. Zhang, S. Tao, B. Wang, and J. Zhao: Proc. SPIE **10091** (2017) 1009110. https://doi.org/10.1117/12.2253753
3 S. D. Gittard and R. J. Narayan: Expert Rev. Med. Devices **7** (2010) 343. https://doi.org/10.1586/erd.10.14
4 P. Patel, B. S. Modi, S. Sheth, and T. Patel: Bonfring Int. J. Ind. Eng. Manag. Sci. **5** (2015) 55. https://doi.org/10.9756/BIJIEMS.8052
5 A. C. Tam, W. P. Leung, W. Zapka, and W. Ziemlich: J. Appl. Phys. **71** (1992) 3515. https://doi.org/10.1063/1.350906
6 M. Von Allmen: J. Appl. Phys. **47** (1976) 5460. https://doi.org/10.1063/1.322578
7 C. E. Yeack, R. L. Melcher, and H. E. Klauser: Appl. Phys. Lett. **41** (1982) 1043. https://doi.org/10.1063/1.93381
8 Y. Cai and N. H. Cheung: Microchem. J. **97** (2011) 109. https://doi.org/10.1016/j.microc.2010.08.001
9 C. C. Ho, Y. J. Chang, J. C. Hsu, C. M. Chiu, and C. L. Kuo: Measurement **80** (2016) 251. https://doi.org/10.1016/j.measurement.2015.10.031

10 A. Stournaras, K. Salonitis, and G. Chryssolouris: Int. J. Adv. Manuf. Technol. **46** (2010) 589. https://doi.org/10.1007/s00170-009-2111-y
11 H. Karasaki, K. Isaji, H. Kinoshita, and M. Kato: Proc. ICALEO (1998) G50, 50–57. https://doi.org/10.2351/1.5059203
12 L. Li, D. J. Brookfield, and W. M. Steen: Meas. Sci. Technol. **7** (1996) 615. https://doi.org/10.1088/0957-0233/7/4/019
13 M. Akhtar, A. Jabbar, N. Ahmed, S. Mehmood, Z. A. Umar, R. Ahmed, and M. A. Baig: Laser Part. Beams **37** (2019) 67. https://doi.org/10.1017/S0263034619000144
14 W. Zhou, K. Li, X. Li, H. Qian, J. Shao, X. Fang, P. Xie, and W. Liu: Opt. Lett. **36** (2011) 2961. https://doi.org/10.1364/OL.36.002961
15 O. A. Nassef and H. E. Elsayed-Ali: Spectrochim. Acta B **60** (2005) 1564. https://doi.org/10.1016/j.sab.2005.10.010
16 A. Elhassan, H. M. Abd Elmoniem, A. K. Kassem, and M. A. Hairth: J. Adv. Res. **1** (2010) 129. https://doi.org/10.1016/j.jare.2010.03.004
17 S. Eschlböck-Fuchs, P. J. Kolmhofer, M. A. Bodea, J. G. Hechenberger, N. Huber, R. Rössler, and J. D. Pedarnig: Spectrochim. Acta B **109** (2015) 31. https://doi.org/10.1016/j.sab.2015.04.009
18 R. Ahmed, A. Jabbar, Z. A. Umar, and M. A. Baig: Plasma Sci. Technol. **23** (2021) 045505. https://doi.org/10.1088/2058-6272/abea70
19 H. Wang, J. Liu, Y. Xu, X. Wang, N. Ren, X. Ren, and Q. Hu: J. Manuf. Process. **62** (2021) 845. https://doi.org/10.1016/j.jmapro.2020.12.051
20 N. Ren, L. Jiang, D. Liu, L. Lv, and Q. Wang: Int. J. Adv. Manuf. Technol. **76** (2015) 735. https://doi.org/10.1007/s00170-014-6293-6
21 Y.-J. Chang, C.-Y. Wang, J.-C. Hsu, C.-C. Ho, and C.-L. Kuo: Measurement **135** (2019) 905. https://doi.org/10.1016/j.measurement.2018.12.042
22 C.-S. Wang, Y.-H. Hsiao, H.-Y. Chang, and Y.-J. Chang: Micromachines **13** (2022) 529. https://doi.org/10.3390/mi13040529
23 Y.-J. Chang, C.-S. Wang, H.-Y. Chang, and Y.-H. Hsiao: Lasers Eng. **57** (2024) 89.

About the Authors

Yuan-Jen Chang received his B.S. degree in mechanical engineering from National Taiwan University, Taiwan, in 1996, his MS degree from the Department of Aeronautics and Astronautics of National Cheng Kung University, Taiwan, in 1998, and his Ph.D. degree in mechanical engineering from the University of Colorado at Boulder, U.S.A., in 2008. He joined the faculty of National Yunlin University of Science and Technology, Taiwan, from 2009 to 2023. He then joined the Graduate Institute of Manufacturing Technology of National Taipei University of Technology in 2023 as a professor. His research interests include semiconductor manufacturing technology, micro-/nanofabrication techniques, EDM, and laser processing.
(yjchang@ntut.edu.tw)

Chau-Shing Wang received his B.S. degree in electrical engineering from National Cheng-Kung University, Tainan, Taiwan, in 1994, and his M.S. and Ph.D. degrees in electrical engineering from the University of Missouri–Columbia, MO, USA, in 1999 and 2003, respectively. He joined the faculty of the Department of Electrical Engineering, National Changhua University of Education, Changhua, Taiwan, in 2003, where he is now a professor. His research interests are in AI, electric power measurement, and LIP detection.
(cswang@cc.ncue.edu.tw)

G. Siva Durga Manikanta received his B.S. degree from Vel Tech Rangarajan Dr. Sagunthala R&D Institute of Science and Technology University, Chennai, India, in 2020 and his M.S. degree from National Yunlin University of Science and Technology, Taiwan, in 2023. (sivadurgamani123@gmail.com)

Yang-Hung Hsiao received his B.S. degree from the Department of Mechanical Engineering of National Yunlin University of Science and Technology, Yunlin, Taiwan, in 2015 and his Ph.D. degree from the Graduate School of Engineering Science and Technology, Yunlin, Taiwan, in 2023. He served as the CEO of AutoCAMTW from 2023. His research interests are in artificial intelligence milling, laser processing, and automated production. (kenny.hsiao@autocamtw.com)